CHAPTER 4

RESULTS AND DISCUSSION

This chapter shows results of experimental and discussion; Sample Synthesis, Microstructure and Chemical Composition Analysis, Crystalline Identification, Micro Hardness, Electrical Resistivity and Seebeck Coefficient, Thermal conductivity, Dimensionless Figure of Merit, Electronic Structure Calculation, Arduino circuits of Bi_2Te_3, Sb_2Te_3 and $Bi_{0.4}Sb_{1.6}Te_{3.4}$ materials and Thermoelectric Sensor and Arduino Application

SAMPLE SYNTHESIS

The basic of experimental procedures were described in our previous study (J.Y. Yang, X.A. Fan, &X.K. Duan, 2006). In brief, Bi and Te powders (<99% purity) were used as stating materials. The powder of Bi, Sb and Te were mixed in planetary ball mill 350 rpm for 10 h under argon atmosphere. The hot press (HP) in a cylindrical graphite die (internal diameter of 4 cm) at 673 K under 60 Mpa for 1 h in vacuum (Yong Soo Lim, Won-Seon Seo, Chang-Won Hwang, 2014) (Xi an Fan, Fan Yang, Guangqiang Li, 2015) (Yun Min Kim, R. Lydia, Kyughan Ahn, 2017). The HP specimen were polished by sand water. The crystal structure of the HP was analyzed by using an X-ray diffractometer (XRD-6100 Shimadzu, Japan) at room temperature using Cu K radiation (= 1.5406 Å) in the range of 20-70° mode. The electrical resistivity and Seebeck coefficient were simultaneously measured using a thermoelectric measurement system (ZEM-3 ADVANCE RIKO) using a helium atmosphere in the temperature range of 273-673 K. The thermal conductivity was calculated by the relation $\kappa = dC_p\lambda$ where d is the density of sample, C_p is the specific heat and λ is thermal diffusivity. The morphology of samples was analyzed by Hitachi-S-3400N Scanning Electron Microscope (SEM) with a secondary electron detector operating in a high vacuum mode with the accelerating voltage 15 kV. The maps of elements distribution were collected using the Energy Dispersive X-ray Spectroscopy by (EDS)

analysis here was performed on a JSM-7800F. The process of fabrication thermoelectric series cell by using Bi_2Te_3 and $Bi_{0.4}Sb_{1.6}Te_{3.4}$ bulk materials. Cutting a Bi_2Te_3 and $Bi_{0.4}Sb_{1.6}Te_{3.4}$ materials were 2×2×2.5 mm^3. And fabricated thermoelectric cell from Bi_2Te_3 materials and used Arduino program for support measurement the value of temperature sensor application.

Bi_2Te_3

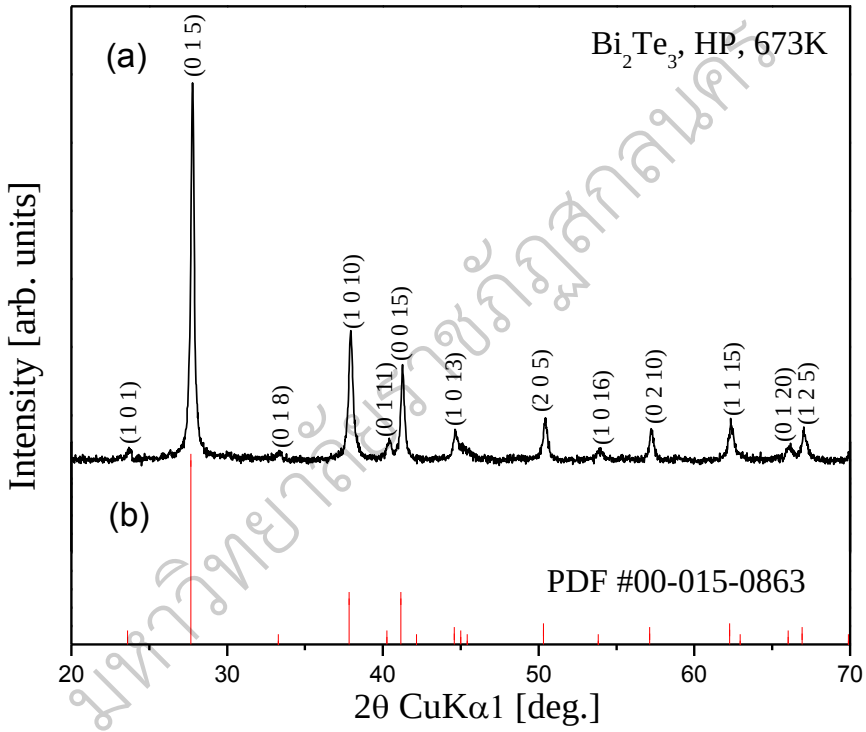

Figure 42 The relationship between diffraction angle and intensity of Bi_2Te_3 bulk

The X-ray diffraction pattern of HP sintered Bi_2Te_3 at room temperature is shown in Fig. 42(a) the relationship between diffraction angle and intensity of x-ray diffraction. The XRD pattern of the sample show the single γ -Bi_2Te_3 phase with an (rhombohedra structure space group in $R\bar{3}m$) in (PDF 00-015-0863). Figure 42(b) shows the diffraction patterns of the Bi_2Te_3 international center for diffraction data reference for a pure Bi_2Te_3 phase (PDF 00-015-0863). The XRD patterns of the

Bi_2Te_3 materials, indicating that pure Bi_2Te_3 crystalline phases were obtained without any impurities. This XRD data is a good for the thermoelectric materials.

Sb_2Te_3

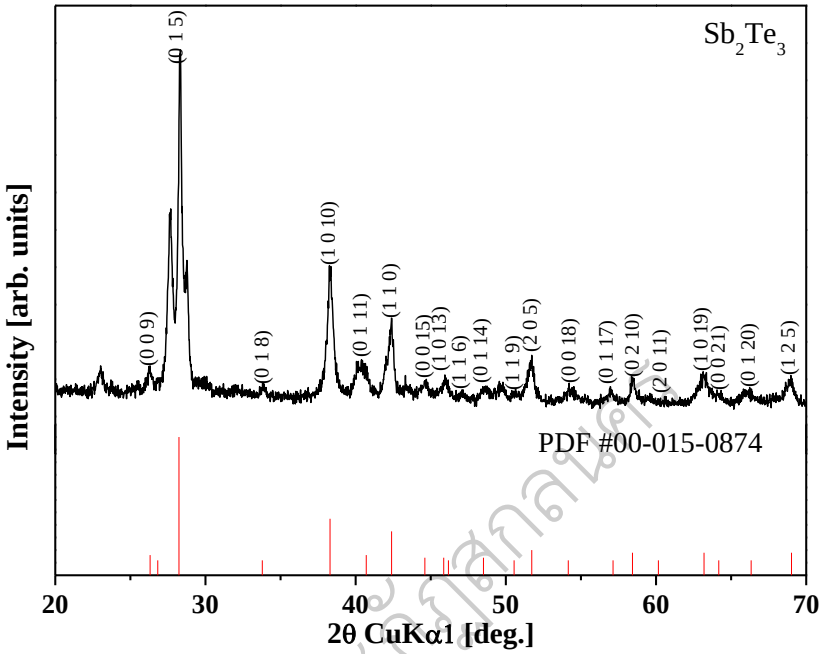

Figure 43 The relationship between diffraction angle and intensity of Sb_2Te_3 bulk

The X-ray diffraction pattern of HP sintered Sb_2Te_3 at room temperature is shown in Fig. 43(a) the relationship between diffraction angle and intensity of x-ray diffraction. The XRD pattern of the sample show the mixed phase an (rhombohedra structure space group in $R-3m$) in (PDF 00-015-0874). Figure 43(b) shows the diffraction patterns of the Sb_2Te_3 international center for diffraction data reference for a pure Sb_2Te_3 phase (PDF 00-015-0874).

$Bi_{0.4}Sb_{1.6}Te_{3.4}$

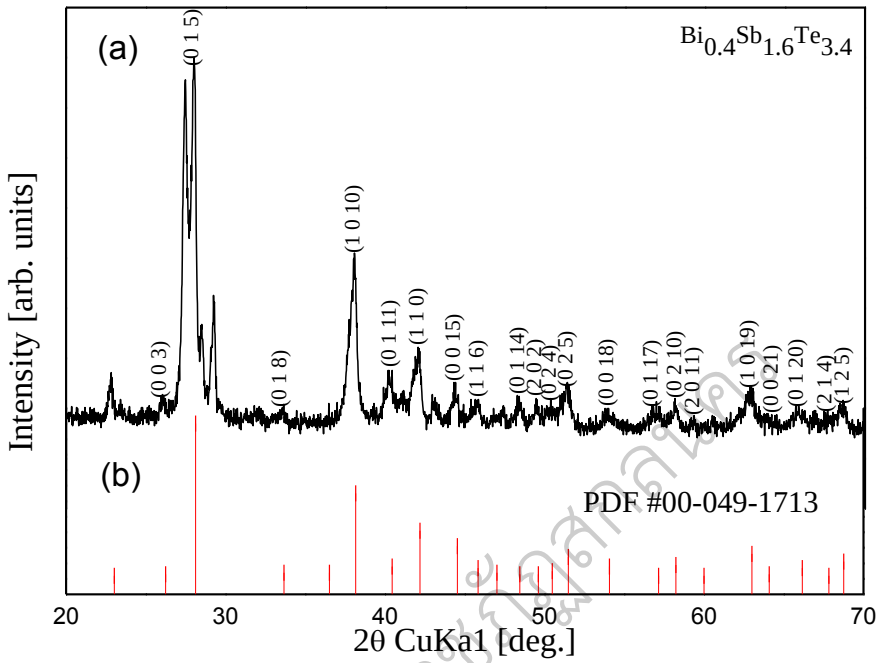

Figure 44 The relationship between diffraction angle and intensity of $Bi_{0.4}Sb_{1.6}Te_3$ bulk

The X-ray diffraction pattern of HP sintered $Bi_{0.4}Sb_{1.6}Te3$ at room temperature is shown in Fig.44(a) the relationship between diffraction angle and intensity of x-ray diffraction. The XRD pattern of the sample show all the diffraction peaks can be indexed according the crystallographic structure of $Bi_{0.4}Sb_{1.6}Te_{3.4}$ (rhombohedra structure space group $R\bar{3}m$) in (PDF 00-049-1713). Figure 44(b) shows the diffraction patterns of the $Bi_{0.4}Sb_{1.6}Te_{3.4}$ international center for diffraction data reference for a pure $Bi_{0.4}Sb_{1.6}Te_{3.4}$ phase (PDF 00-049-1713). The XRD patterns of the $Bi_{0.4}Sb_{1.6}Te_{3.4}$ materials, indicating that pure $Bi_{0.4}Sb_{1.6}Te_{3.4}$ crystalline phases were obtained without any impurities.

MICROSTRUCTURE AND CHEMICAL COMPOSITION ANALYSIS

The microstructure of Bi_2Te_3 and $Bi_{0.4}Sb_{1.6}Te_{3.4}$ bulk sample were investigated and analyzed by Scanning Electron Microscope (Hitachi-S-3400N). The microstructure details, including the morphology, size, and crystallinity of the fabricated Bi_2Te_3 materials. Figure 4.2 (a) shows the morphology of the as-prepared Bi_2Te_3 powder, which had an uneven distribution of particles, size 5. Fig. 4.2(b-c) shows Bi_2Te_3 and $Bi_{0.4}Sb_{1.6}Te_{3.4}$ bulk samples, after sintered by HP method.

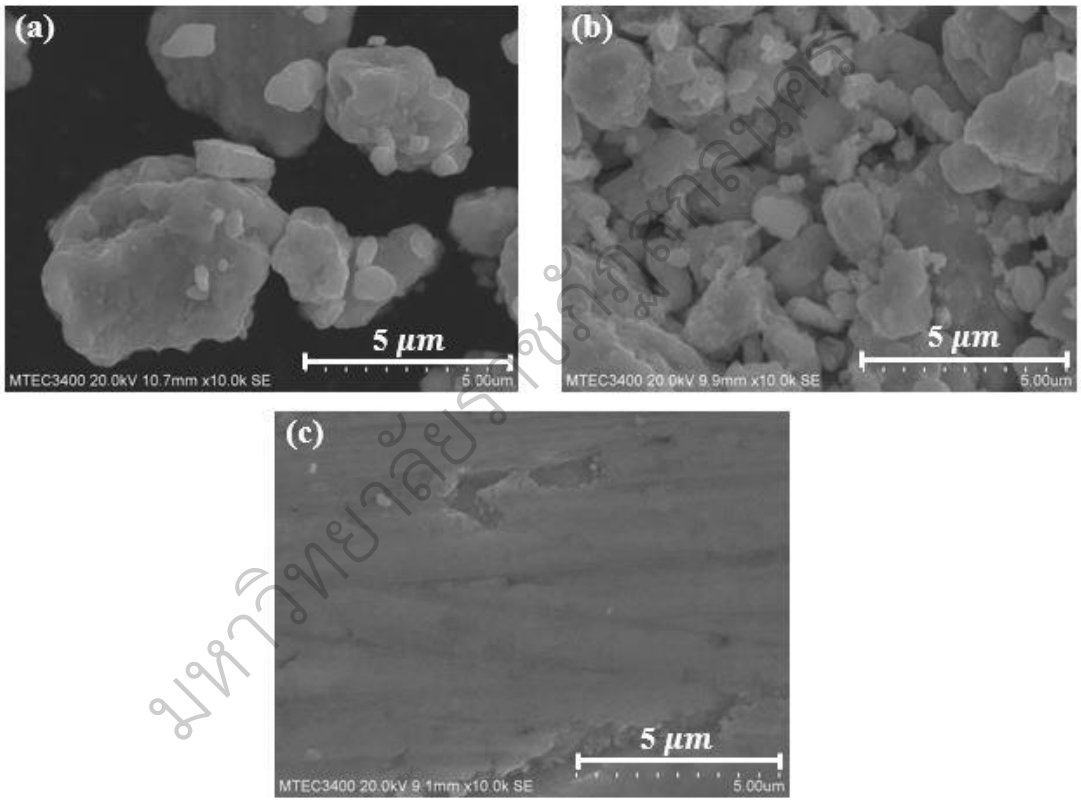

Figure 45 SEM micrographs for (a) Bi-Te powder (b) B_2Te_3 and (c) $Bi_{0.4}Sb_{1.6}Te_{3.4}$ bulk particles prepared by a hot-pressing method (bar = 5 μm)

Energy Dispersive X-ray Spectroscopy

Bi_2Te_3

Energy Dispersive X-ray Spectroscopy is an analytical technique used for the elemental analysis or chemical characterization. The characteristic spectrum of X-rays emitted by the specimen after excitation by high-energy electrons to obtain information about its elemental composition. For EDX analysis here was performed on a JSM-7800F Prime. For EDX analysis here was performed on a JSM-7800F Prime. Map of Bi, Te, and O elements distribution collected for the polished surface of Bi_2Te_3 sample as shown in Fig.46.

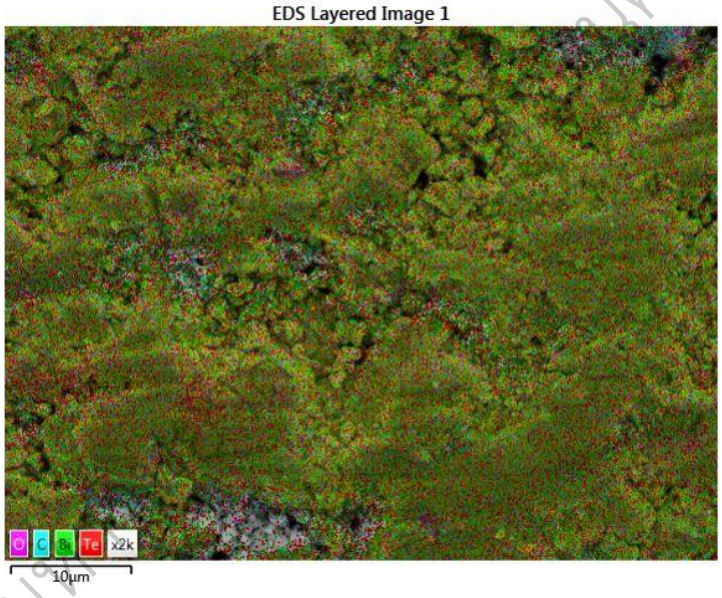

Figure 46 Mapping of Bi_2Te_3 bulk

Bright, areas/points corresponding to pores, the green points was Bi, red/Te and purple/O for investigate. The distribution of elements in Bi_2Te_3 sample were looks different. Bi and Te were distribution of disorganized as show Fig. 47.

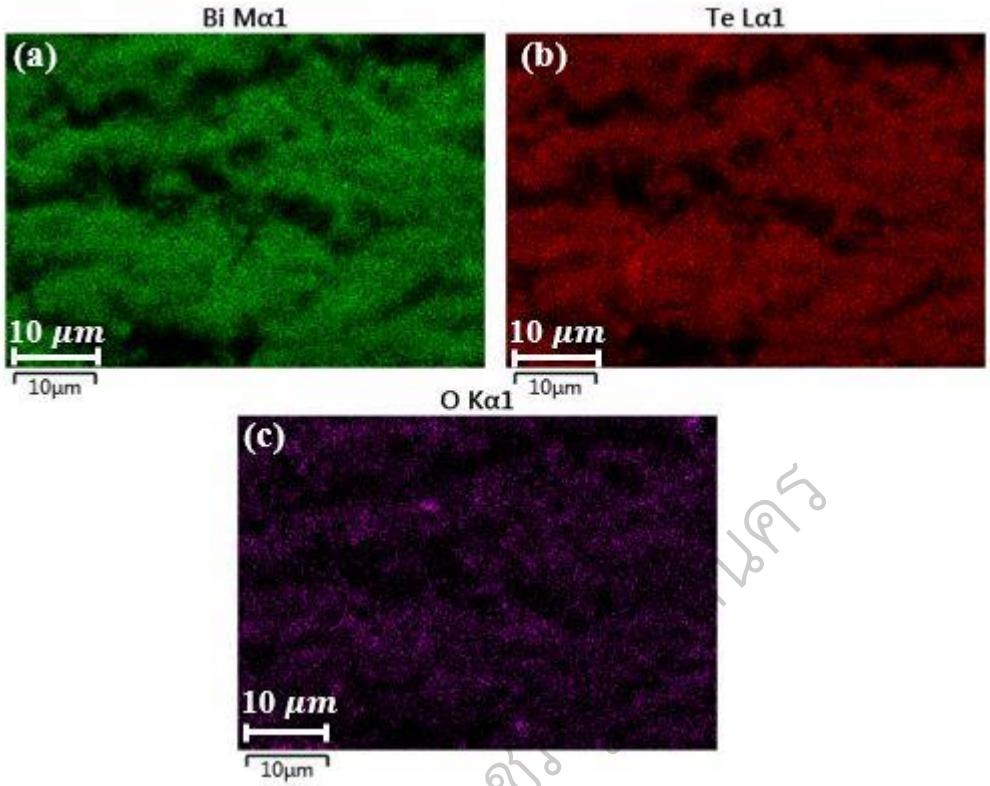

Figure 47. The comparison of EDX maps for Bi_2Te_3 bulk (a) map of Bi (b) map of Te and (c) map of O bulk

$Bi_{0.4}Sb_{1.6}Te_{3.4}$

The EDS technique of Bi, Sb, Te, and O elements distribution collected for polished surface of $Bi_{0.4}Sb_{1.6}Te_{3.4}$ sample as shown in Fig.48 Bright, areas/points corresponding to pores yellow /Bi, green/Sb, red/Te and blue/O for investigate.

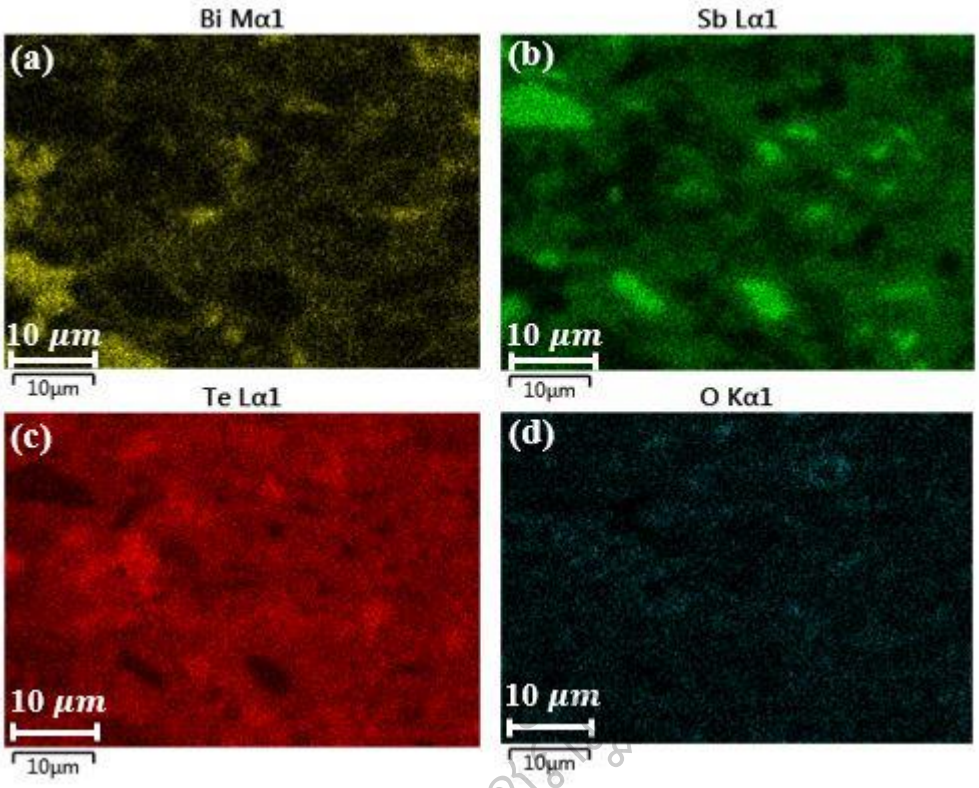

Table 48 The comparison of EDX maps for $Bi_{0.4}Sb_{1.6}Te_{3.4}$ bulks (a) map of Bi (b) map of Sb and (c) map of Te and (d) map of O bulk

CRYSTALLINE IDENTIFICATION

Figure 49 shows hexagonal lattice parameter of the sintered Bi_2Te_3 and $Bi_{0.4}Sb_{1.6}Te_{3.4}$ sample with compare the literature data. The lattice parameter a and c determined from XRD patterns of the γ –Bi_2Te_3 and $Bi_{0.4}Sb_{1.6}Te_{3.4}$ phase. The result show that the lattice parameter a and c of sample. The value of Bi_2Te_3 sample was show lattice parameter are a = 0.4315 nm and c = 3.0443 nm, and $Bi_{0.4}Sb_{1.6}Te_{3.4}$ sample are a = 0.4487 and 3.1877 nm. However, these values are lower than that of the sample of (Natl et al,.1964, Ritter, J et al,. 1997), but Bi_2Te_3 and $Bi_{0.4}Sb_{1.6}Te_{3.4}$ sample has lattice parameter value similar literature data.

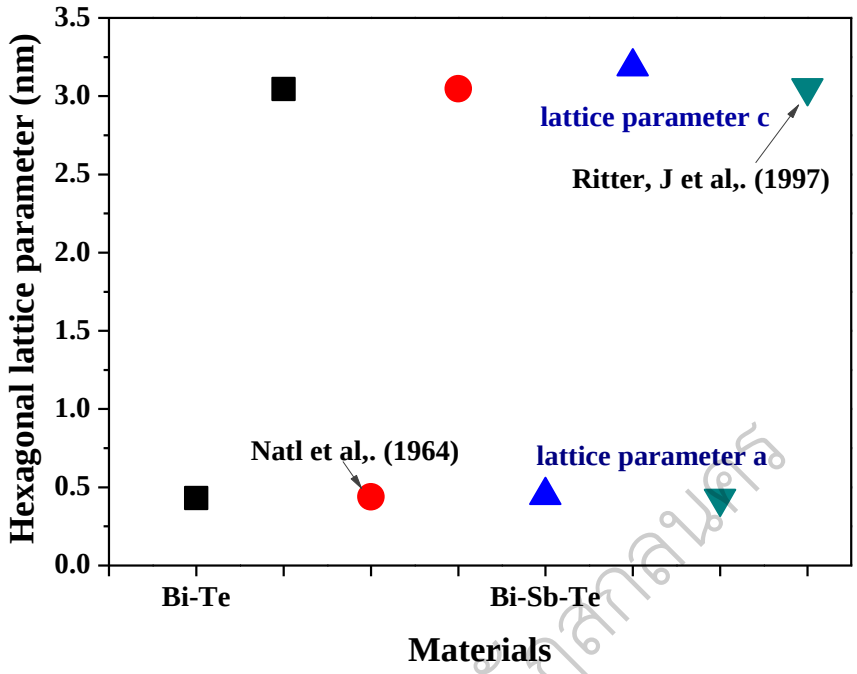

Figure 49 Hexagonal lattice parameter of the sintered Bi_2Te_3 and $Bi_{0.4}Sb_{1.6}Te_{3.4}$ bulk

MICRO HARDNESS

The Vickers hardness (H_V) was measured by Micro hardness tester. The applied load of 0.245, 0.490, 0.980, 2.942 and 9.807 N respectively with loading time 10 s show in Fig. 50

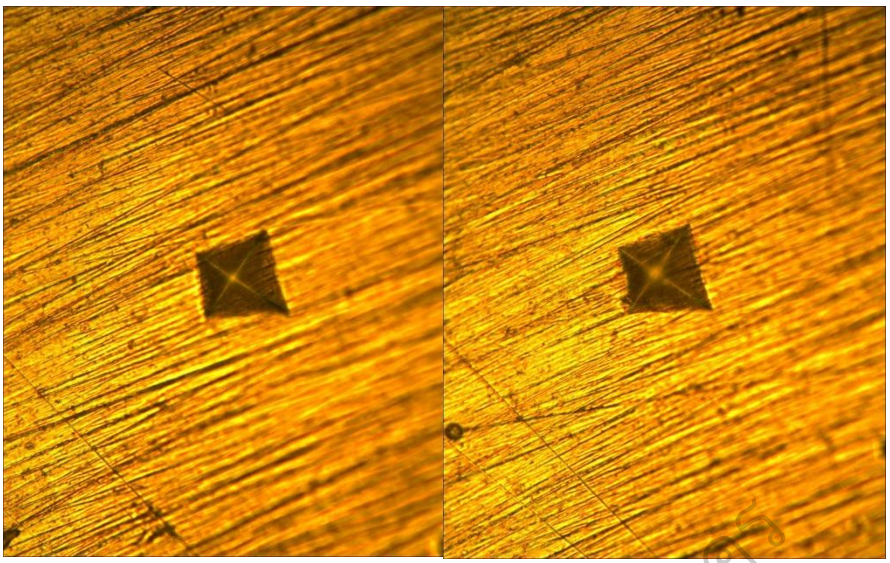

Figure 50 shows pressing of Bi_2Te_3 and $Bi_{0.4}Sb_{1.6}Te_{3.4}$ sample from the micro hardness tester.

Bi_2Te_3

The (H_V) values of Bi_2Te_3 and $Bi_{0.4}Sb_{1.6}Te_{3.4}$ samples were measured in room temperature and the average hardness measured data. The relationship between the Micro Vickers hardness (H_V) and load for the sample, as shown in Fig. 51. The (H_V) values of the Bi_2Te_3 and $Bi_{0.4}Sb_{1.6}Te_{3.4}$ sample were measured at room temperature and calculated the standard deviation. The applied load of 0.245, 0.490, 0.980, 1.961, 2.942, 4.903 and 9.807 N respectively and the loading time of 10 s. The maximum hardness values of Bi_2Te_3 sample and calculated standard deviation of the sintered sample is 55.8 ± 1.2, 51.1 ± 1.8, 49.1 ± 3.8, 47.8 ± 4.1, 52 ± 2.4, 48 ± 4.2 and 45.3 ± 9.7 GPa respectively. The maximum hardness values of $Bi_{0.4}Sb_{1.6}Te_{3.4}$ sample is

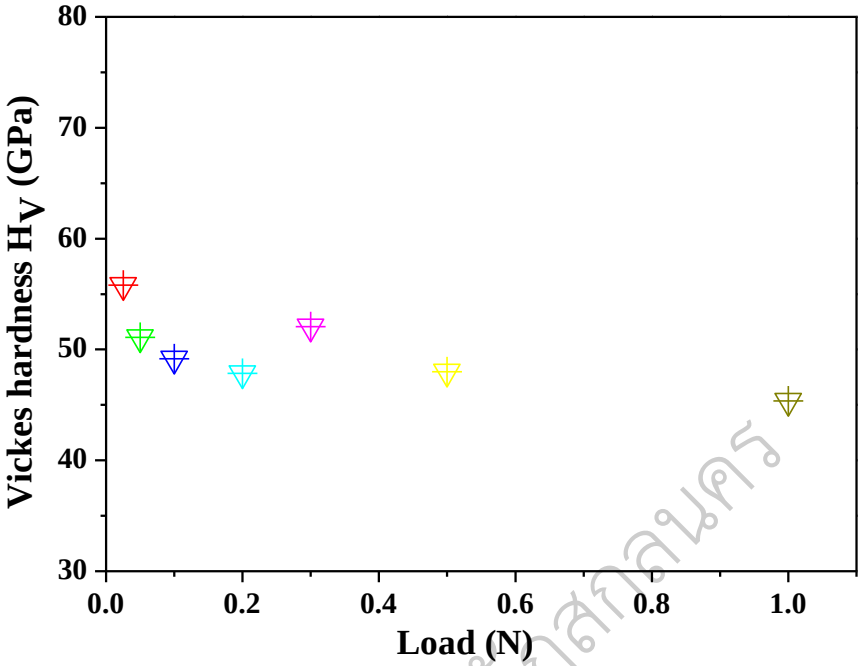

Fig 51 The relationship between the Micro Vickers hardness and applied load for Bi_2Te_3 bulk

$Bi_{0.4}Sb_{1.6}Te_{3.4}$

The Vickers hardness (H_V) was measured by Micro hardness tester. The applied load of 0.245, 0.490, 0.980, 2.942 and 9.807 N respectively with loading time 10 s show in Fig.52. The maximum hardness values of $Bi_{0.4}Sb_{1.6}Te_{3.4}$ sample and calculated standard deviation of the sintered sample is 26.8 ± 3.2, 37.6 ± 3.18, 43.1 ± 1.9, 52.3 ± 3.9, 38.8 ± 5.8, 43.1 ± 2.5 and 42.6 ± 7.37 GPa respectively

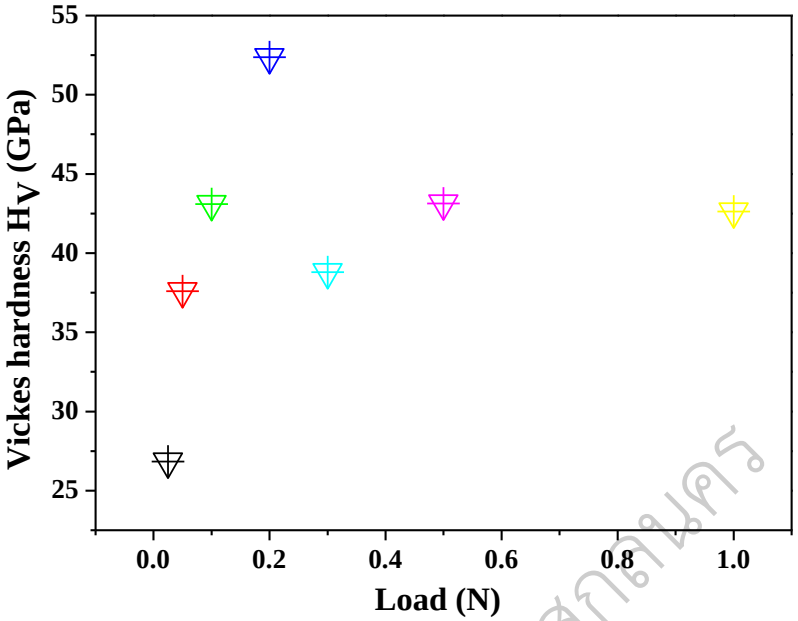

Fig 52 The relationship between the Micro Vickers hardness and applied load for $Bi_{0.4}Sb_{1.6}Te_{3.4}$ bulk

Table 3 the mechanical properties of Bi_2Te_3 and $Bi_{0.4}Sb_{1.6}Te_{3.4}$ bulk

Sample	Lattice Parameter		Bulk Density	Theoretical Density	Relative Density	Vickers Hardness	Elastic constant
	a (nm)	*C* (nm)	(g/cm^3)	(g/cm^3)	(g/cm^3)	(GPa)	
Bi_2Te_3	0.4315	3.04437	6.20	7.42	82.21	49.90	0.043
$Bi_{0.4}Sb_{1.6}Te_{3.4}$	0.4487	3.18733	6.07	7.32	82.92	39.2	0.021

ELECTRICAL RESISTIVITY AND SEEBECK COEFFICIENT

Bi_2Te_3

Figure 53 Temperature dependence of the electrical resistivity (ρ) for sintered Bi_2Te_3 sample, together with the literature data from Go-Eun Lee et al.,2014. The ρ were measured in the temperature range of 325 – 525 K. The ρ of Bi_2Te_3 sample was decreased with increasing temperature indicate of semiconductor behavior. The ρ values of the Bi_2Te_3 sample are 20.347 x $10^{-5}\Omega$ m at 325 K to 13.8878 x $10^{-5}\Omega$ m at 525 K respectively. However, these values are hight than that of the samples of Go-Eun Lee et al.,2014

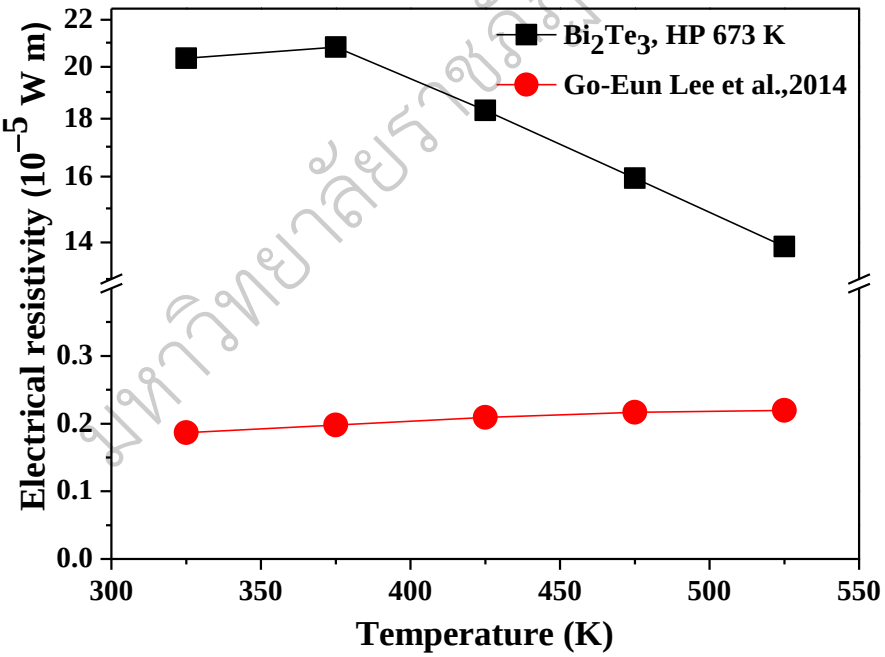

Figure 53 Temperature dependence of the electrical resistivity for sintered Bi_2Te_3 bulk

Figure 54 shown the temperature dependence of the Seebeck coefficient (S) of the Bi_2Te_3 sample were prepare hot-press at 673 K for 1 h in argon atmosphere and compared with literature data. The S were measured in the temperature range of 325 – 525 K. The S of Bi_2Te_3 shown negative value indicate that an n-type. The S value of sample was decreases with increasing temperature from -155.920 μV K^{-1} at 325 K to -123.65 μV K^{-1} at 525 K respectively. However, these values are hight than that of the samples of Go-Eun Lee et al.,2014

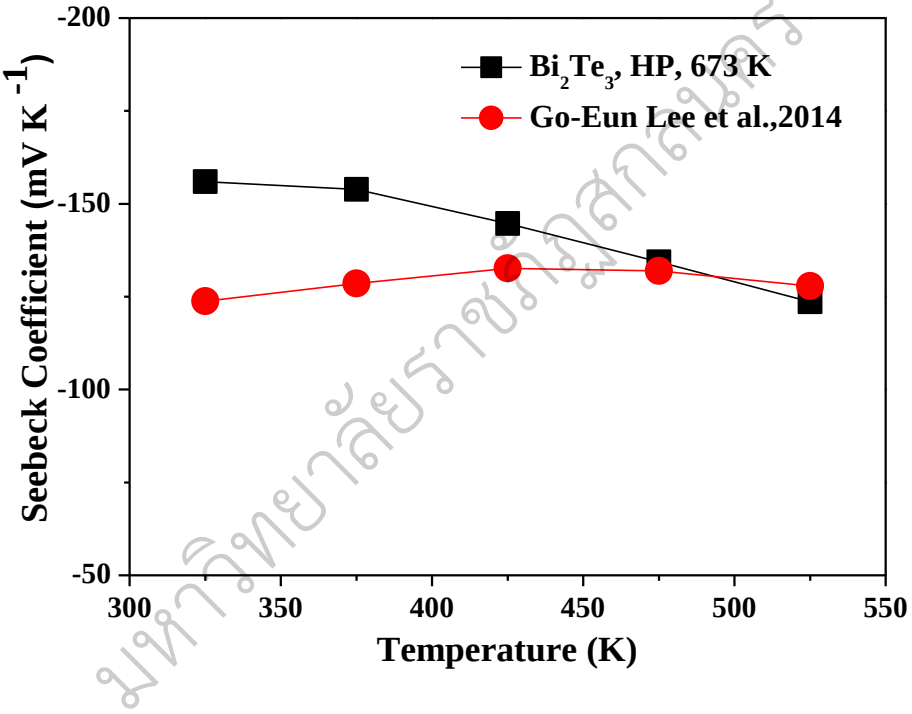

Figure 54 Temperature dependence of the Seebeck coefficient for sintered Bi_2Te_3 bulk

Figure 55. Temperature dependence of the power factor (PF) for sintered Bi_2Te_3 sample. together with the literature data from Go-Eun Lee et al.,2014. The power factor of sample were evaluated by S and ρ value as equation $\frac{S^2}{\rho}$. The PF were measured in the temperature range of 325 – 525 K. The PF of Bi_2Te_3 sample was increased with increasing temperature. The PF values of the Bi_2Te_3 sample are 1.041 × 10^{-4} W m^{-1} K^{-2} at 325 K to 1.1106 × 10^{-4} W m^{-1} K^{-2} at 525 K.

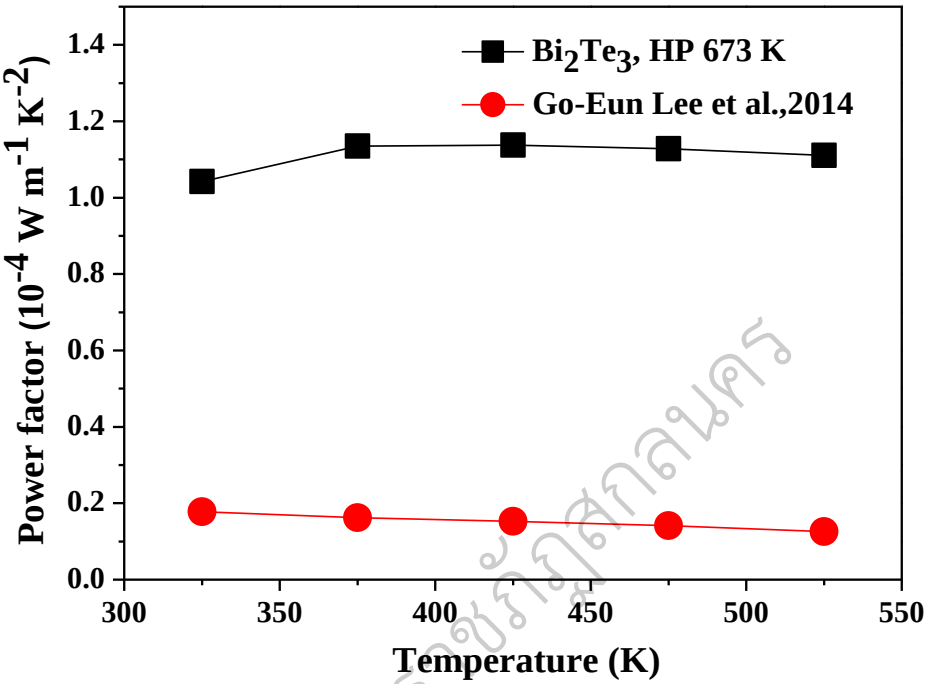

Figure 55 Temperature dependence of the power factor for sintered Bi_2Te_3 bulk

$Bi_{0.4}Sb_{1.6}Te_{3.4}$

Figure 56 shows the temperature dependence of the of the $Bi_{0.4}Sb_{1.6}Te_{3.4}$ sample were prepared hot-press at 673 K for 1 h in argon atmosphere and compared with literature data. The S were measured in the temperature range of 325 – 525 K. The S of $Bi_{0.4}Sb_{1.6}Te_{3.4}$ shown positive value indicate that an p-type. The S value of sample was increases with increasing temperature from 156.3379 μV K^{-1} at 325 K to 159.0197 μV K^{-1} at 375 K after that was decreases with increasing temperature. However, these values are lower than that of the samples of Yum Min Kim et al.,2017, but $Bi_{0.4}Sb_{1.6}Te_{3.4}$ has Seebeck coefficient value similar like literature data.

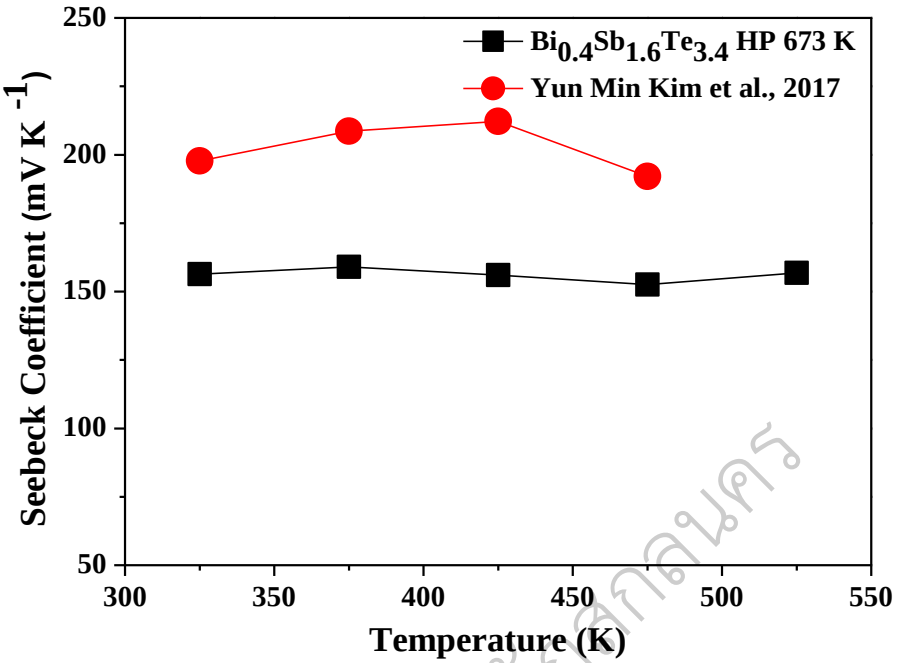

Figure 56 Temperature dependence of the Seebeck coefficient for sintered $Bi_{0.4}Sb_{1.6}Te_{3.4}$ bulk

Figure 57 shows temperature dependence of the ρ for sintered $Bi_{0.4}Sb_{1.6}Te_{3.4}$ sample, together with the literature data from Yum Min Kim et al.,2017. The ρ were measured in the temperature range of 325 – 525 K. The ρ of $Bi_{0.4}Sb_{1.6}Te_{3.4}$ sample was increased with increasing temperature indicate of semiconductor behavior. The ρ values of the $Bi_{0.4}Sb_{1.6}Te_{3.4}$ sample are 0.044 mΩ at 325 K to 0.051 mΩ at 525 K respectively. However, these values are lower than that of the samples of Yum Min Kim et al.,2017

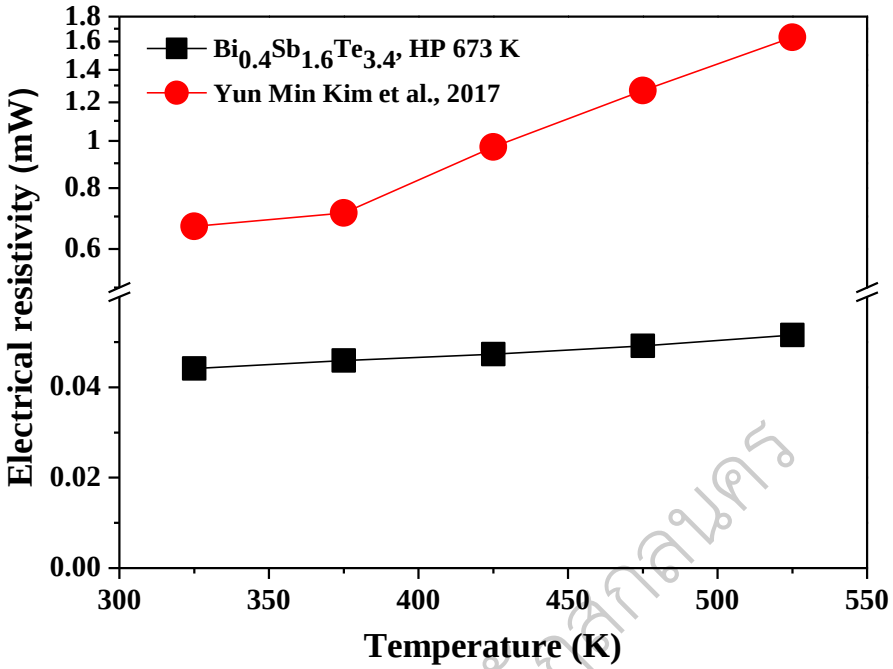

Figure 57 Temperature dependence of the electrical resistivity for sintered $Bi_{0.4}Sb_{1.6}Te_{3.4}$ bulk

Figure 58 shows temperature dependence of the PF for sintered $Bi_{0.4}Sb_{1.6}Te_{3.4}$ sample. together with the literature data from Yum Min Kim et al.,2017. The PF were measured in the temperature range of 325 – 525 K. The PF of $Bi_{0.4}Sb_{1.6}Te_{3.4}$ sample was decreased with increasing temperature. The PF values of the $Bi_{0.4}Sb_{1.6}Te_{3.4}$ sample are 0.055 mW m^{-1} K^{-2} at 325 K to 0.035 mW m^{-1} K^{-2} at 525 K.

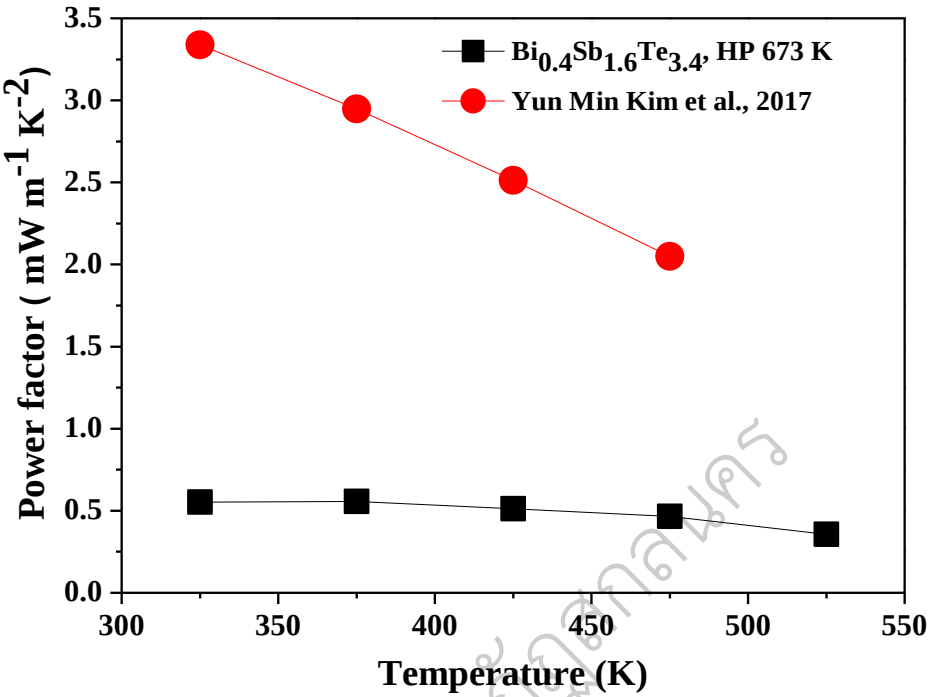

Figure 58 Temperature dependence of the power factor for sintered $Bi_{0.4}Sb_{1.6}Te_{3.4}$ bulk

THERMAL CONDUCTIVITY

Bi_2Te_3

Figure 59 shows temperature dependence of the thermal conductivity (κ) for sintered Bi_2Te_3 sample, together with the literature data. The κ were measured in the temperature range of 325 – 475 K. The κ of sample was calculation equation $\kappa = \alpha C_p d$. The κ of Bi_2Te_3 sample was increased with increasing temperature. The κ values of the Bi_2Te_3 sample are 1.8493 W m^{-1} K^{-1} at 325 K to 2.3579 W m^{-1} K^{-1} at 475 K. However, the thermal conductivity of Bi_2Te_3 values have higher than that of literature data. The κ values of the Bi_2Te_3 sample have lower than that other semiconductor its means Bi_2Te_3 materials have a good thermoelectric property.

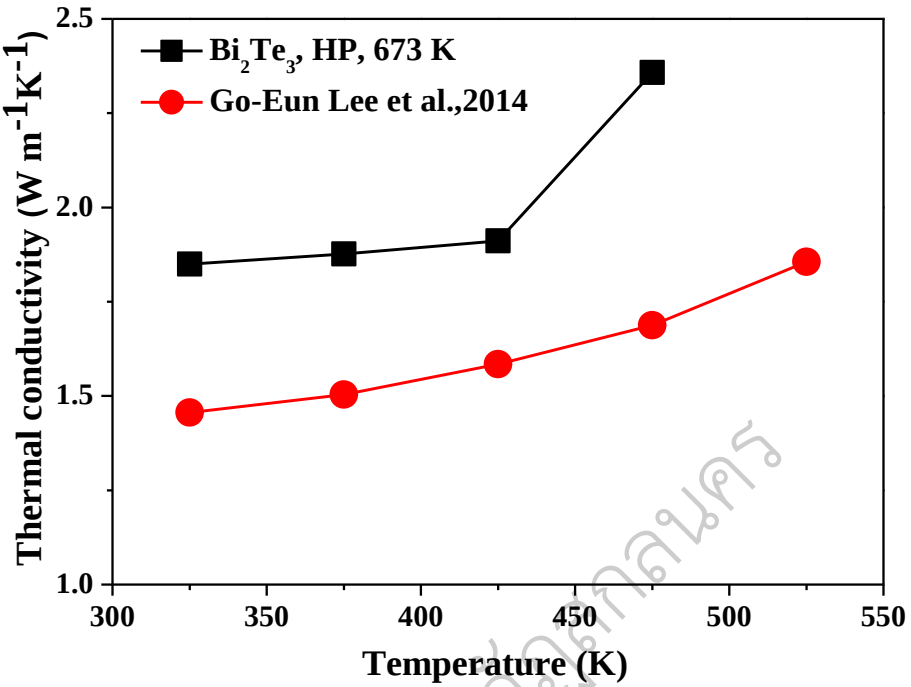

Figure 59 Temperature dependence of the thermal conductivity for sintered Bi_2Te_3 bulk

$Bi_{0.4}Sb_{1.6}Te_{3.4}$

Figure 60 shows temperature dependence of the κ for sintered $Bi_{0.4}Sb_{1.6}Te_{3.4}$ sample, together with the literature data. The κ were measured in the temperature range of 325 – 475 K. The κ of $Bi_{0.4}Sb_{1.6}Te_{3.4}$ sample was increased with increasing temperature. The κ values of the $Bi_{0.4}Sb_{1.6}Te_{3.4}$ sample are 2.0089 W m^{-1} K^{-1} at 325 K to 2.0528 W m^{-1} K^{-1} at 475 K.

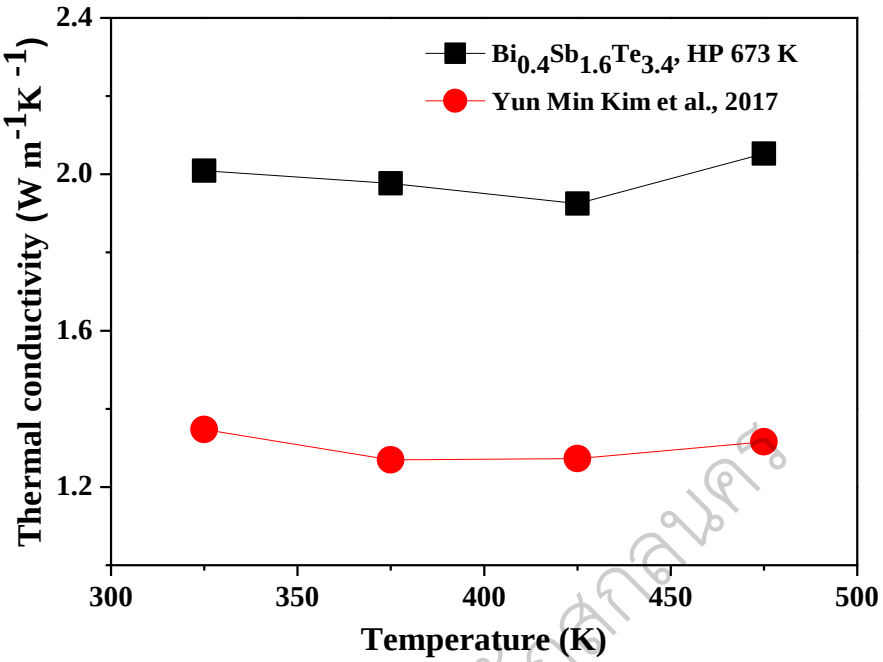

Figure 60 Temperature dependence of the thermal conductivity for sintered $Bi_{0.4}Sb_{1.6}Te_{3.4}$ bulk

DIMENSIONLESS FIGURE OF MERIT

Bi_2Te_3

The dimensionless figure of merit *(ZT)* was calculated by using the above–mentioned values of the Seebeck coefficient (S), electrical resistivity (ρ) and thermal conductivity (κ) according to the relation;

$$ZT = \frac{S^2 T}{\rho \kappa}$$

Figure 61 shows temperature dependence of the dimensionless figure of merit (*ZT*) for sintered Bi_2Te_3 sample, together with the literature data. The *ZT* were measured in the temperature range of 325 – 475 K. The *ZT* of Bi_2Te_3 sample was increased with increasing temperature but lower than that literature data over the

whole temperature range. The *ZT* values of Bi_2Te_3 sample are 0.018 at 325 K to 0.025 at 475 K.

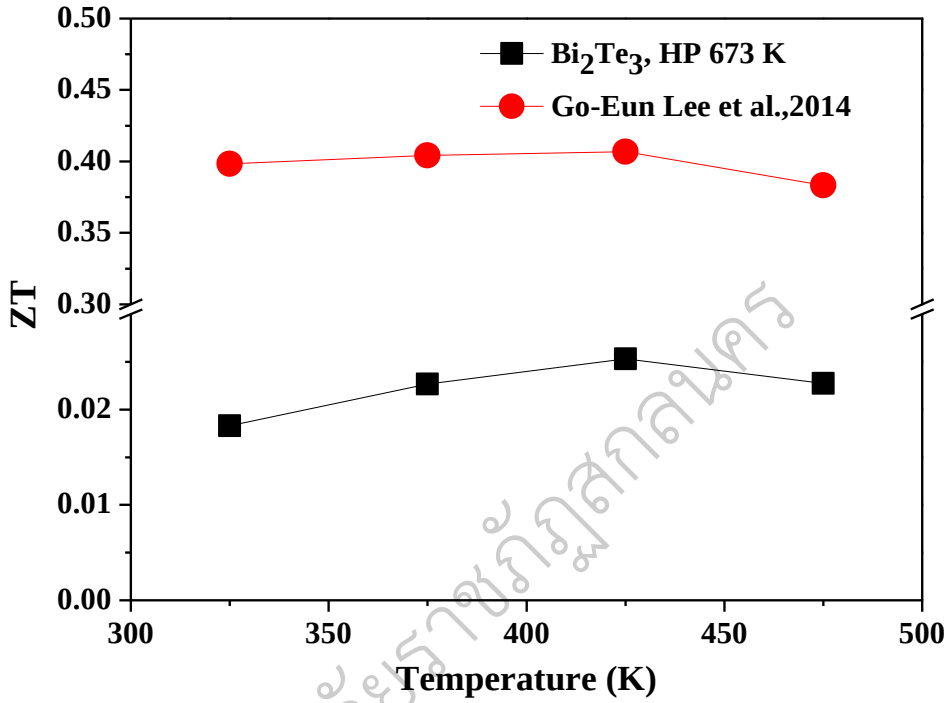

Figure 61 Temperature dependence of the dimensionless figure of merit for sintered Bi_2Te_3 bulk

$Bi_{0.4}Sb_{1.6}Te_{3.4}$

Figure 62 shows temperature dependence of the *ZT* for sintered $Bi_{0.4}Sb_{1.6}Te_{3.4}$ sample, together with the literature data. The *ZT* were measured in the temperature range of 325 – 475 K. The *ZT* of $Bi_{0.4}Sb_{1.6}Te_{3.4}$ sample was increased with increasing temperature. The *ZT* values of $Bi_{0.4}Sb_{1.6}Te_{3.4}$ sample are 0.089 at 325 K to 0.107 at 475 K.

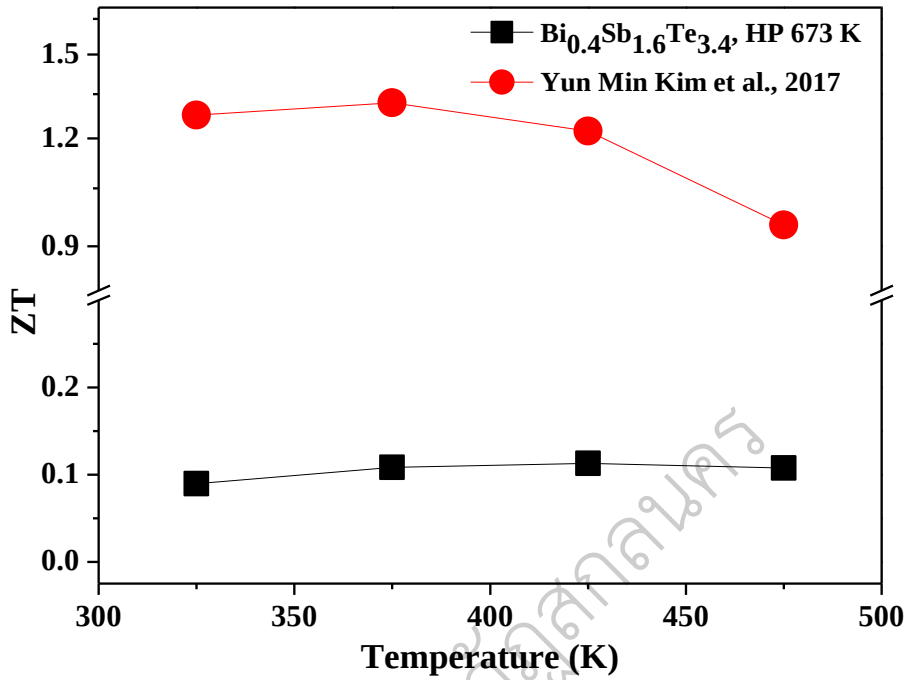

Figure 62 Temperature dependence of the dimensionless figure of merit for sintered $Bi_{0.4}Sb_{1.6}Te_{3.4}$ bulk

ELECTRONIC STRUCTURE CALCULATION

The electronic structure calculation was performed using the density functional theory and BoltzTraP simulation. For the Bi_2Te_3 and $Bi_{2-x}Sb_xTe_3$ cluster models were designed by sing space group number 166, lattice parameter a = 4.38 Å, b = 4.38 Å and c = 30.49 Å, as show Fig. 63.

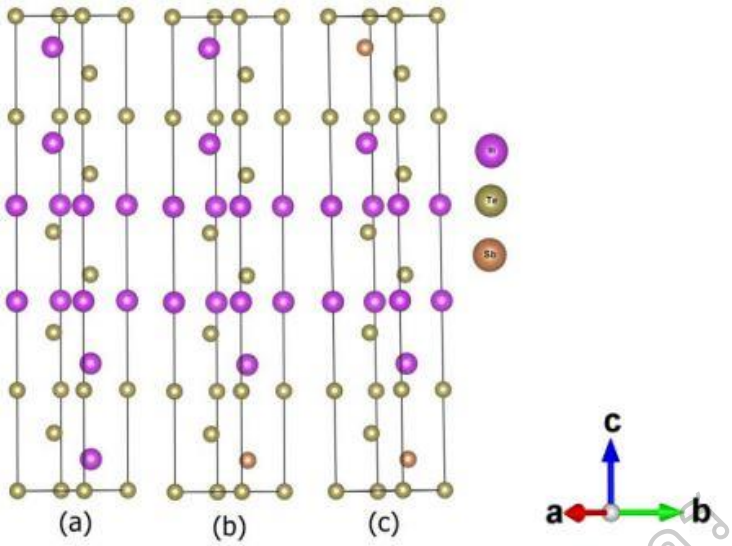

Figure 63 Cluster atom model *(a)* Bi_2Te_3, *(b)* $Bi_{1.67}Sb_{0.33}Te_3$, and *(c)* $Bi_{1.33}Sb_{0.67}Te_3$

The electronic structure was calculated by the density functional theory based on QUANTUM ESPRESSO B.Y. Yavorsky, N.F.Hinsche, I. Mertig, P. Zahn, (2011) The exchange correlation function, energy convergence limit set as 10^{-8} Ry, and energy cutoff 40 Ry are performed *(J. P. Perdew, K. Burke and M. Ernzerhof, 1996).* The density of states was calculated using 8×8×1 k –mesh and k –points in the Brillion zone. The thermoelectric properties, such as, Seebeck coefficient, electrical conductivity, and thermal conductivity was calculated using Boltzmann transport theory based on BoltzTraP (K.H.M. Georg, D. J. Singh, (2006, T.J. Scheidemantel, C. Ambrosch–Draxl, T. Thonhauser, J.V. Badding, J.O. Sofo, 2003), the equation can be written as;

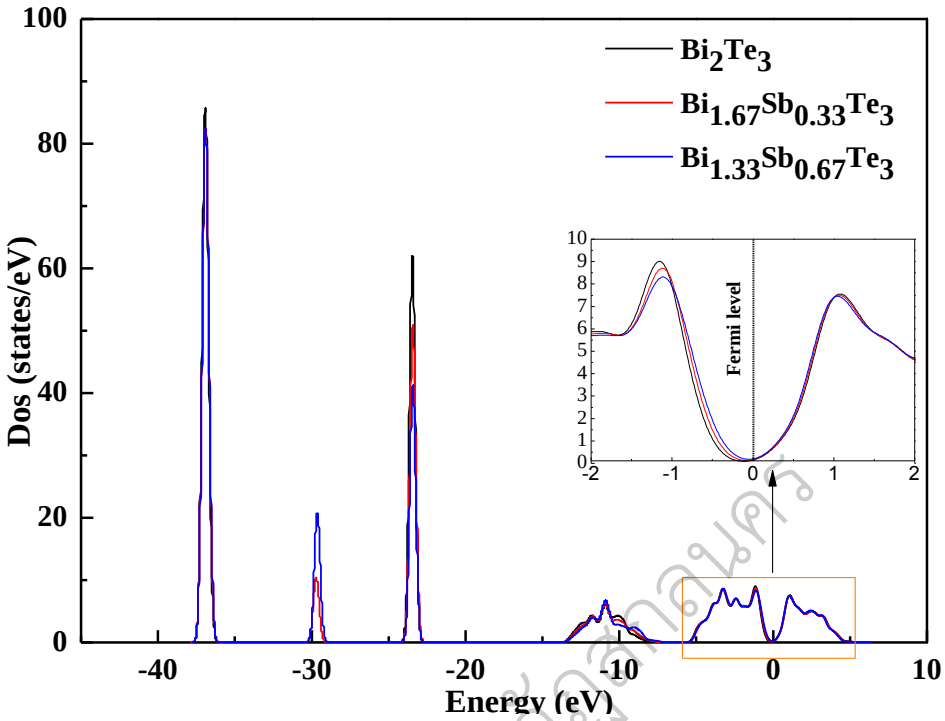

Fig. 64 Total density of states of $Bi_{2-x}Sb_xTe_3$ (x=0, 0.33, 0.67)

The total density of states of $Bi_{2-x}Sb_xTe_3$ (0, 0.33, and 0.67) are show in Fig. 64 The formation energy of $Bi_{2-x}Sb_xTe_3$ (x = 0, 0.33, 0.67) as shown in Table 1. Both results show semiconductor behavior composed of electron and hole motive, which effected to thermoelectric properties.

Table 4 The formation energy of $Bi_{2-x}Sb_xTe_3$ (x=0, 0.33, 0.67)

Formation energy	Bi_2Te_3(Ry)	$Bi_{1.67}Sb_{0.33}Te_3$(Ry)	$Bi_{1.33}Sb_{0.67}Te_3$(Ry)
Total energy	-100048.04	-9617.47	-9186.90
Total all-electron energy	-380673.68	-350575.03	-320476.37
One-electron contribution	-1281.75	-1314.63	-1347.50
Hartree contribution	771.13	785.60	800.06
XC contribution	-657.69	-674.83	-691.96

Formation energy	Bi_2Te_3(Ry)	$Bi_{1.67}Sb_{0.33}Te_3$(Ry)	$Bi_{1.33}Sb_{0.67}Te_3$(Ry)
Ewald contribution	−1648.60	−1648.60	−1648.60
One−center paw	−7231.13	−6765.02	−6298.92
Contribution			

ARDUINO CIRCUITS OF Bi_2Te_3 AND $Bi_{0.4}Sb_{1.6}Te_{3.4}$ MATERIALS.

Thermoelectric Cell

The result of different temperature with voltage value for thermoelectric cell is shown in Fig. 65. The voltage has increased with increasing temperature which a maximum of 0.03 mV at 49 K per 1 pair compare with commercial.

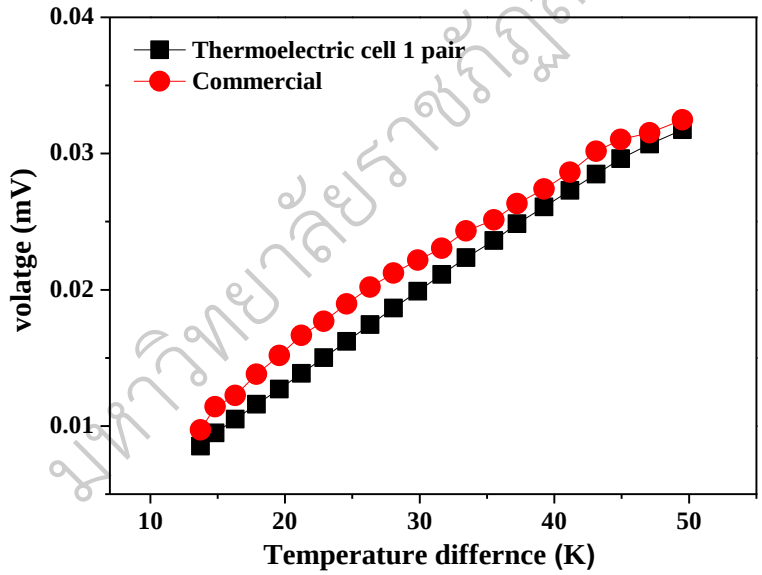

Figure 65 The voltage of the device at different temperature difference

Figure 66 shows the electrical power value from thermoelectric cell at different temperature difference. The electrical power has increased with increasing temperature. The maximum value of electrical power is 0.9 mW at temperature difference around 47 K per 1 pair compare with commercial.

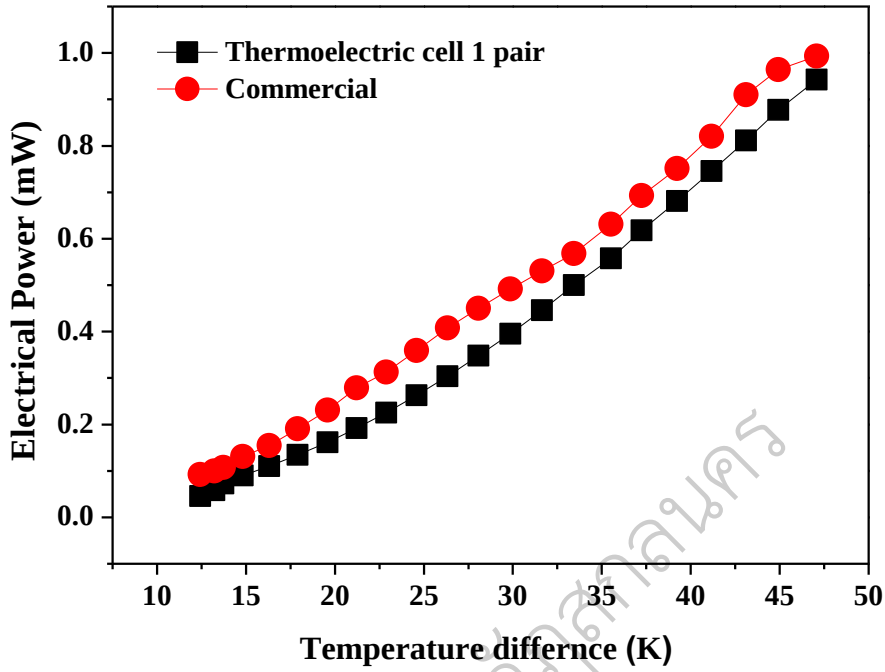

Fig. 66 The electrical power of the device at different temperature difference

Thermoelectric Sensor and Arduino Application

The thermoelectric series cell fabricated by using p–$Bi_{0.4}Sb_{1.6}Te_{3.4}$ and n– Bi_2Te_3 bulk materials. The Bi_2Te_3 and $Bi_{0.4}Sb_{1.6}Te_{3.4}$ materials cut size of 2.5×2.5×3 mm^3 for making series cell. The TE cell was constructed by connecting in series with zinc electrodes for connected p– $Bi_{0.4}Sb_{1.6}Te_{3.4}$ and n– Bi_2Te_3 materials. and using advanced ceramic tubes size 10 cm3 was a body of the temperature sensor as show in Fig.67(a). ESP8266 module was an impressive, low cost WI–FI module suitable for adding WI–FI functionality to an existing microcontroller project via a UART serial connection. In the case, used the ESP8266 module and using Arduino program were supported. The selection board Arduino for the working process of the program as show in Fig.67(b).

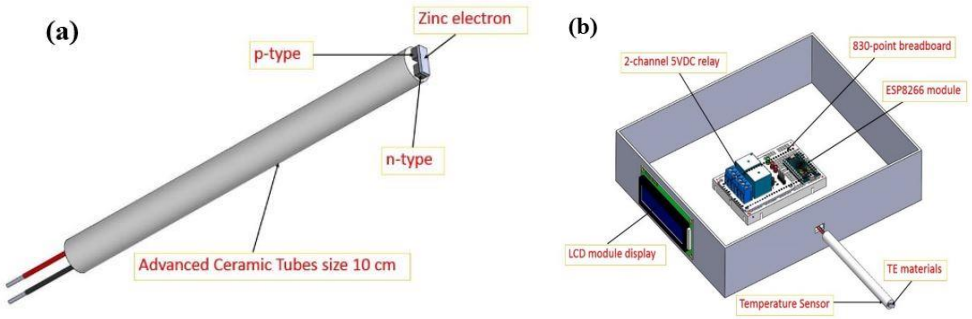

Figure 67 (a) System of working temperature sensor (b) Diagram of temperature sensor

ESP8226 operated voltage of 3.3 – 3.6 V which the compatible with other sensors using 5V. The maximum active module current is 200 mA, frequency is 40 MHz for this system and used ESP8266 receiver from thermoelectric cell. After that the voltage converted signal to be temperature by controller transmitter and send to phone or display in this program as shown that in Fig. 68.

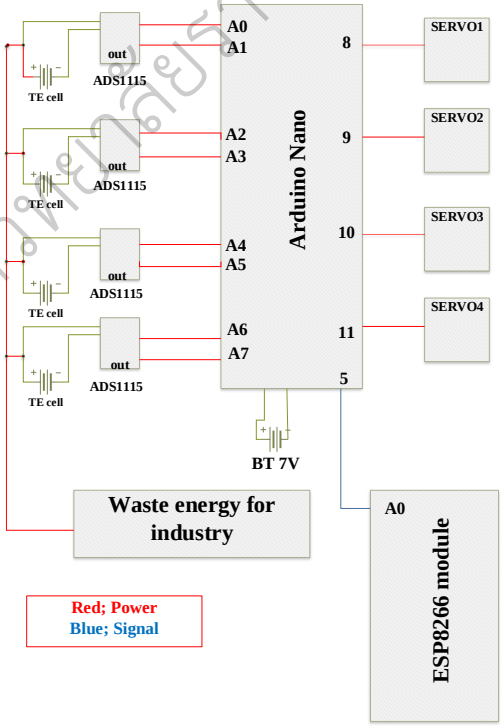

Figure 68 Flow map of power and signal through circuit by Visio Professional

Figure 69 shows the relationship between temperature with time. The temperature sensor compared with thermocouple type K. The temperature sensor value has similar thermocouple type K. Due to the TE materials p and n type were slightly different the TE properties. As a result, the output signal was a little error.

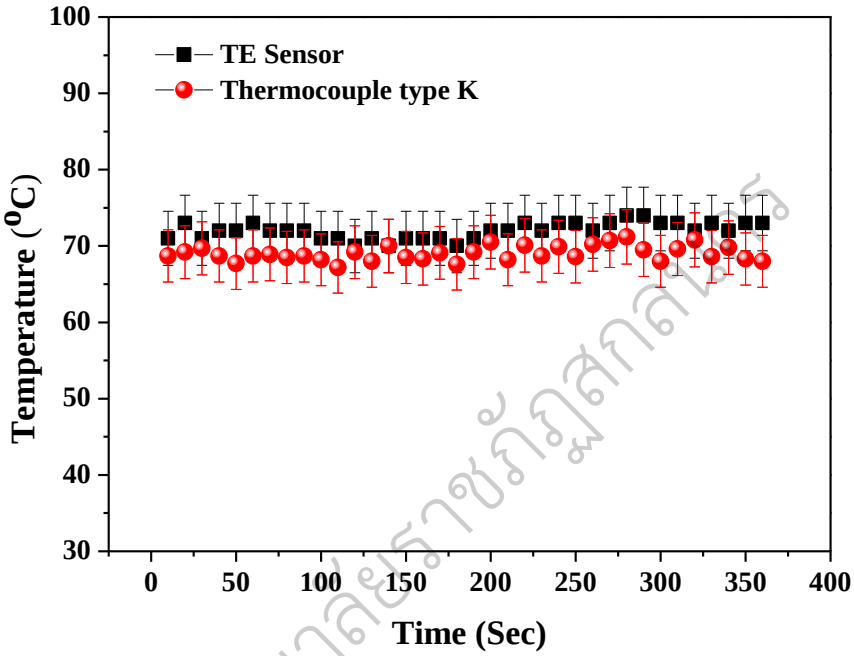

Figure 69 The relationship between temperature with time of TE sensor